

## Novel analysis of single crystal René N5 superalloy

### Characterization of high-temperature corrosion and particle analysis with the Apreo ChemiSEM

#### Authors

Alice Scarpellini and Roger Maddalena

#### Introduction

Nickel-based superalloys are a class of high-performance materials with exceptional mechanical properties, even at high temperatures, as well as excellent corrosion, oxidation, and creep resistance. Because of this, these superalloys are primarily used in components that operate in extreme environments such as gas turbines and aircraft engines. Beyond nickel, these alloys consist of various elements such as chromium, cobalt, and/or molybdenum; the high-temperature strength and creep resistance are attributed to the presence of solid solution strengthening.

This application note explores the properties and behavior of single-crystal René N5, a Ni-based superalloy used in aircraft engines, particularly the corrosion and damage mechanisms that occur during high-temperature creep. The Thermo Scientific™ Apreo™ ChemiSEM supported this characterization with seamless integration between imaging, energy-dispersive X-ray spectroscopy (EDS), and particle analysis.

#### Materials and challenges

The René N5 superalloy is most often used in turbine blades, which operate in the hot zone of aircraft engines. Two pieces of the alloy were first subjected to a high-temperature isothermal or non-isothermal creep test; microstructural changes were then examined.

Alloy (wt%)	Ni	Cr	Co	Mo	W	Al	Ta	Hf	Re	C
René N5	Bal.	7.0	7.5	1.5	5.0	6.2	6.5	0.15	3.0	0.25

Table 1. Nominal composition of the René N5 superalloy analyzed in this study.

In the isothermal creep test, temperature was maintained at 1,100°C to simulate extreme working conditions. For the non-isothermal test, the piece underwent a thermal cycle with a set point of 900°C and several ramps to 1,100°C, which better simulates actual service conditions that contain take-off and changes in altitude. Figure 1 shows the two different thermal treatments during the creep tests.

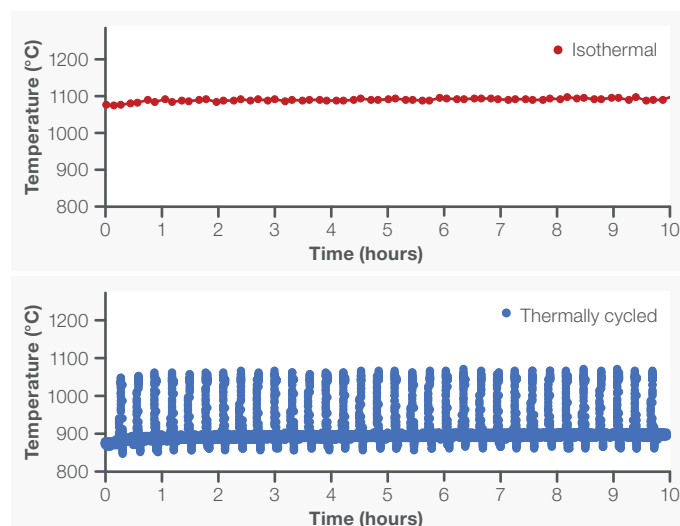


Figure 1. Graphs of time vs. temperature for a portion of the creep tests.

The strain measured during the creep tests is shown in Figure 2, indicating that the isothermal material had less strain over the first 150 hours, exhibiting ultimate failure after 177 hours. The thermally cycled material, meanwhile, showed a higher strain within the same period, but fractured much later, after 262 hours. Strain percentages for both tests are shown in Table 2.

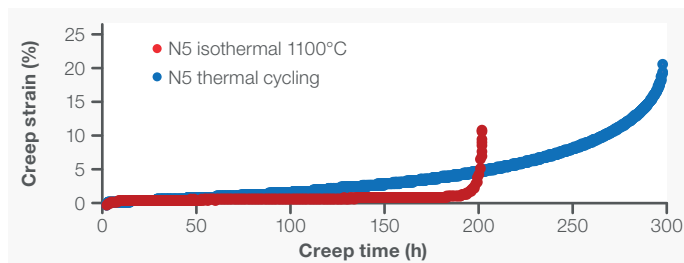


Figure 2. Creep strain percentage vs hours, measured on both the isothermal and thermally cycled samples.

	Isothermal (hours)	Thermal cycle (hours)
1% strain	122	39
2% strain	172	94
3% strain	174	130
Rupture	177	262

Table 2. Creep test results for the tested superalloy samples.

Following these tests, both post-mortem pieces were embedded in resin and polished to expose a cross section (Figure 3).

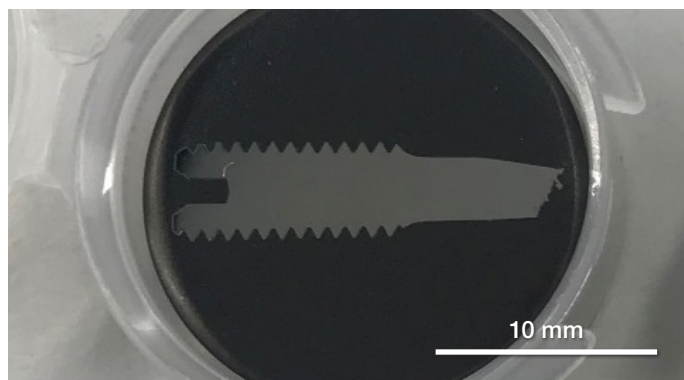


Figure 3. Image of a thermally cycled test piece in resin, mounted and polished.

Comprehensive material characterization, consisting of scanning electron microscopy, EDS, and automated particle analysis, was used to better understand the degradation mechanism of René N5. With this approach, the Apreo ChemiSEM is capable of providing invaluable insights into the nature of the superalloy, including analysis of its metallic phases, surface corrosion, and quantification of the carbides and pores found in the material.

### Imaging with scanning electron microscopy

Electron microscopy imaging provides an initial overview of the material. Thermo Scientific™ ChemiSEM™ Technology allowed for EDS analysis to be integrated into the imaging workflow, providing simultaneous imaging and chemical analysis. However, for the sake of clarity, SEM and EDS results will be discussed separately in this application note.

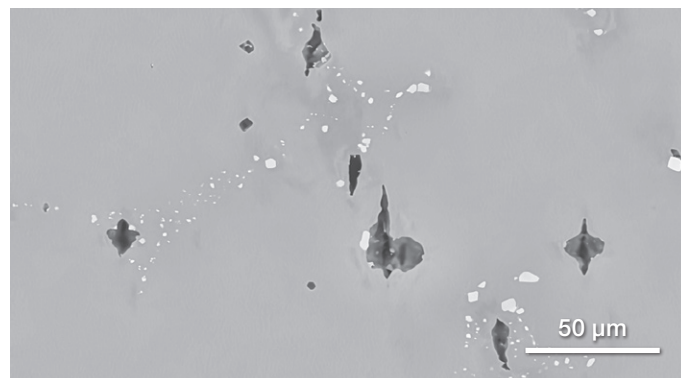


Figure 4. Backscattered electron image showing the distribution of pores within the superalloy sample along with their shapes and sizes, as well as the presence of precipitates.

Figure 4 shows a low-magnification overview of the surface, confirming the presence of carbides (bright areas) and pores (dark areas). Irregularly shaped pores suggest that deformation or damage was accumulated during the experiment.

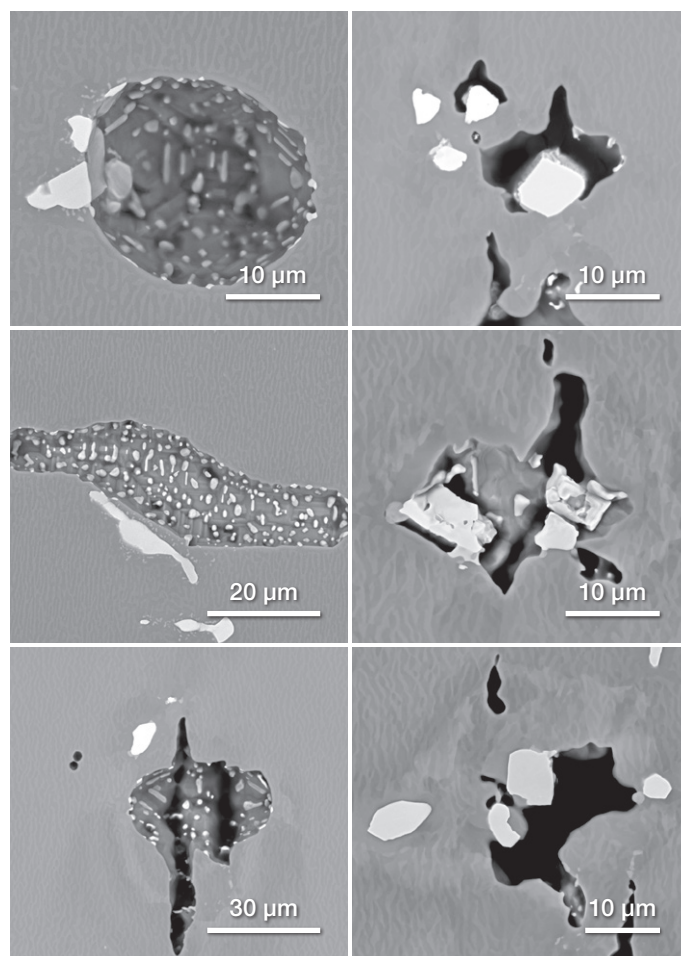


Figure 5. Close up views of some of the pores and precipitates found across the surface of both thermally cycled and isothermal samples.

The higher magnification views in Figure 5 highlight the presence of precipitates inside the cavity of the pores as well as in the surrounding dense metal. Both the precipitates and pores were present before the thermal experiment; while the shape of the precipitates was likely not affected by external forces, the pores may have become elongated or irregularly shaped during testing.

### Chemical characterization

Understanding the distribution of alloy phases in René N5 is important as they influence the alloy's mechanical properties. Two metallic face-centered cubic (fcc) phases form the alloy matrix; the  $\gamma$  phase is an ordered fcc phase, whereas the  $\gamma'$  phase is a disordered fcc phase. As shown in Figure 6,  $\gamma$  and  $\gamma'$  phases are visible as tiger stripes in the backscattered electron (BSE) image. Brighter precipitates can also be seen.

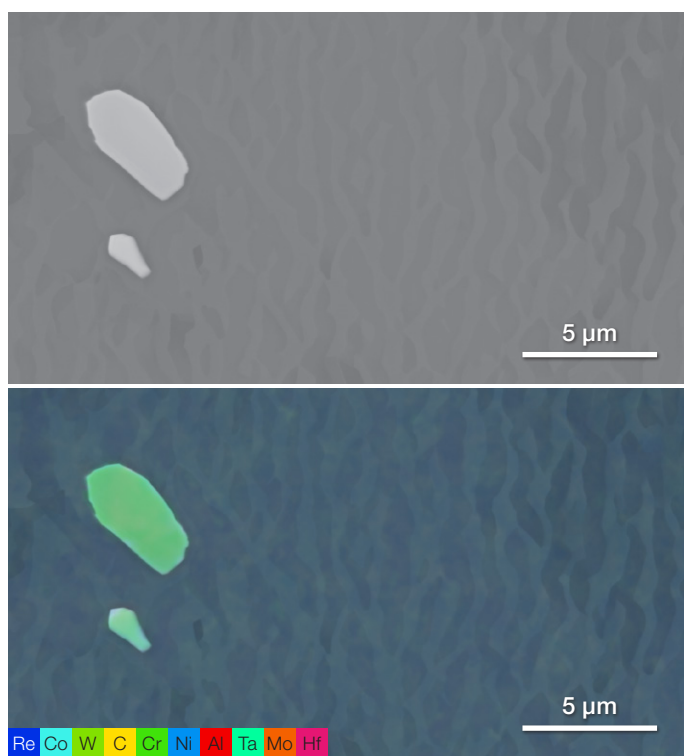


Figure 6. Imaging and ChemiSEM characterization of the isothermal sample.

BSE imaging alone cannot determine the number of metallic phases or their area fractions. Quantitative EDS mapping, meanwhile, is insufficient for determining the exact composition of each unique phase. Manually analyzing each phase is also unreliable, as variation in BSE video level can lead to errors. This is why we have introduced ChemiPhase, a real-time, automated phase analysis component in ChemiSEM Technology. ChemiPhase performs a single data acquisition and analysis, eliminating the need for additional software and data processing. It also does not require any prior knowledge of the chemistry of the different phases in order to perform its analysis.

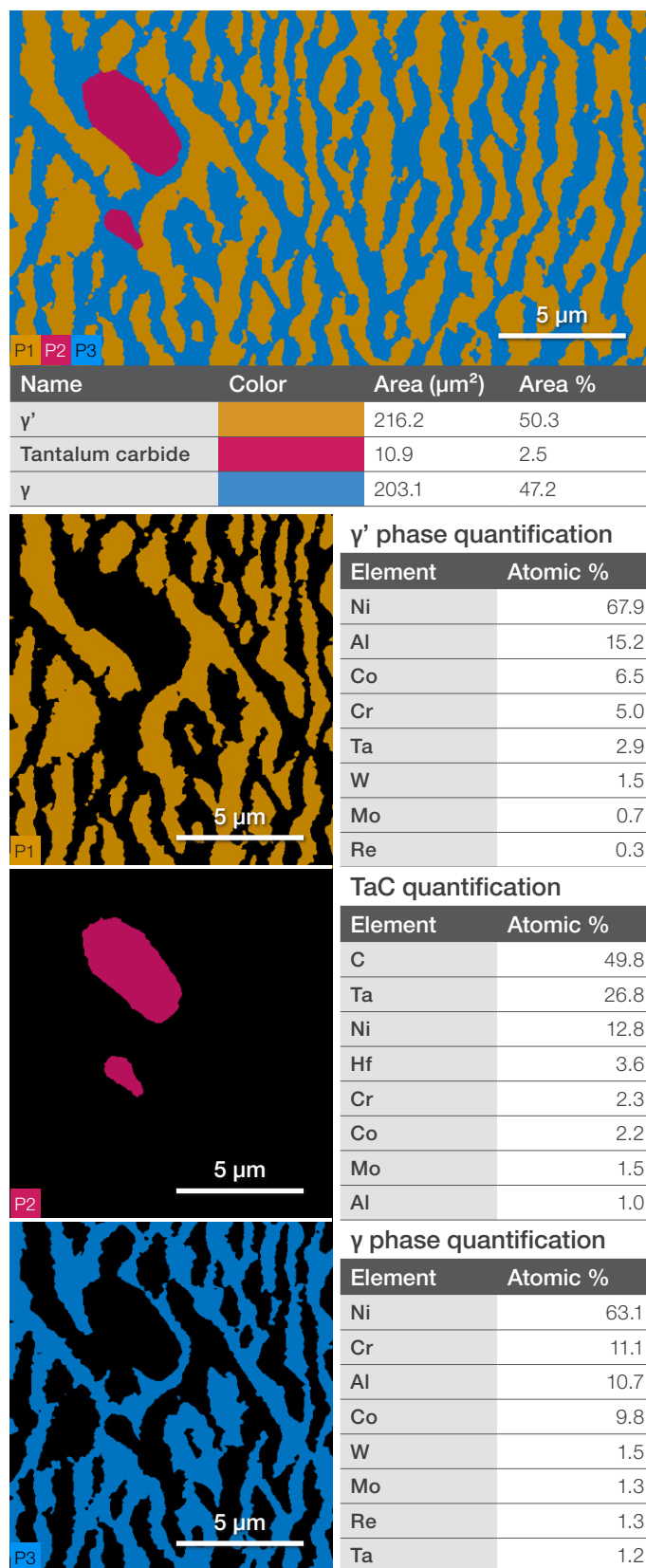


Figure 7. Single acquisition ChemiPhase characterization of the bulk René N5 superalloy. ChemiPhase was able to determine the distribution of different materials found in the field of view, together with the corresponding spectra (shown in Figure 8) and quantification.



Figure 7 shows the ChemiPhase characterization of the isothermal sample. Although the distribution of  $\gamma$  and  $\gamma'$  phases could potentially be differentiated in the compositional contrast obtained with the T1 detector, accurately quantifying their composition would have necessitated multiple region or point analyses, yielding less precise results. Additionally, determining their area fractions would have required additional image processing, which could be prone to errors.

ChemiPhase provided the location, area fraction, composition, and spectrum for each of the identified phases. The comparison in Figure 8 emphasizes the minimal chemical disparity between the two primary alloy phases.

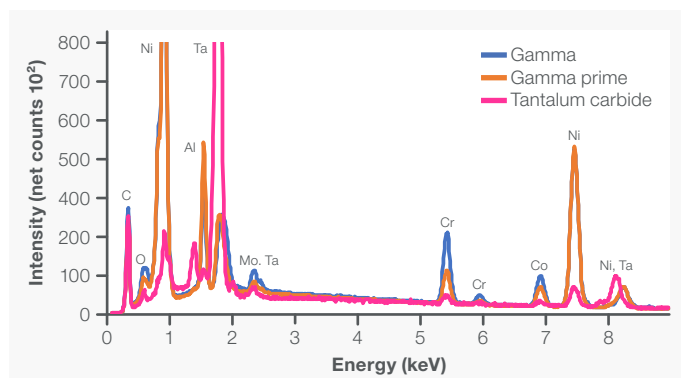


Figure 8. Spectra comparison between the  $\gamma$  and  $\gamma'$  phases highlights the relatively small compositional difference between the two phases. Data extracted from the ChemiPhase characterization.

The precipitates observed in the isothermal sample were identified as tantalum carbides (TaC), as evident from the quantification of the corresponding phase (P2) in Figure 7. Both samples contain populations of TaC particles as well as chromium carbides, as shown in the thermally cycled sample (P3, dark blue) in Figure 9.

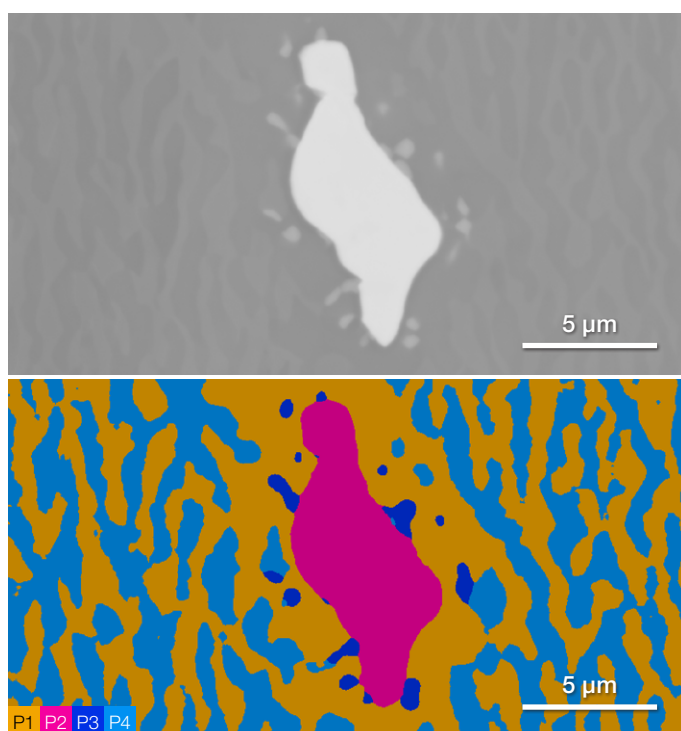


Figure 9. ChemiPhase characterization of the thermally cycled sample.

Monitoring changes in the  $\gamma$  and  $\gamma'$  phases can provide critical insights into the behavior and performance of nickel-based superalloys under various conditions. Thanks to ChemiPhase, this characterization was achieved within a single data acquisition, providing a complete set of information with no need for additionally data processing.

### Surface oxidation

The characterization of surface oxidation is a crucial step in nickel-based superalloys research. Both samples show heavily oxidized and irregular surfaces along with the presence of various carbides, nitrides, and oxides (Figure 10). Darker contrast given by the T1 detector suggests a low mean atomic number near the surface.

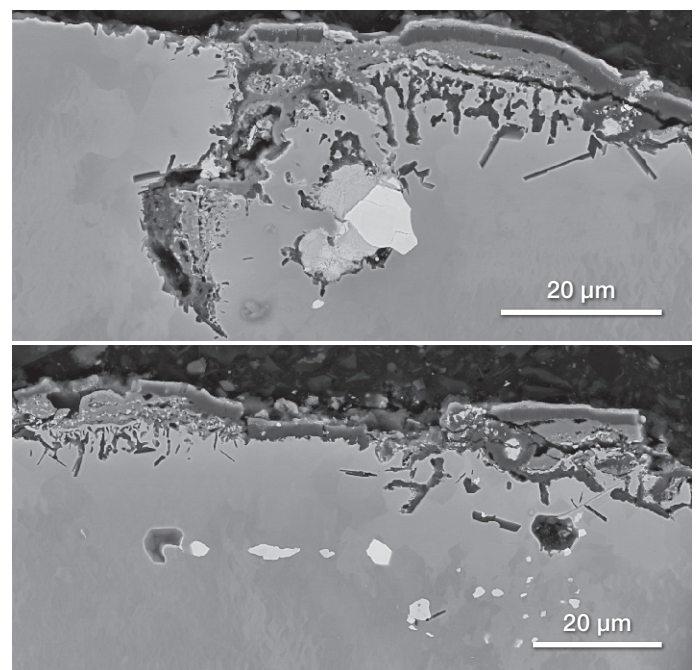


Figure 10. SEM images of the oxidized surface of the thermally cycled sample.

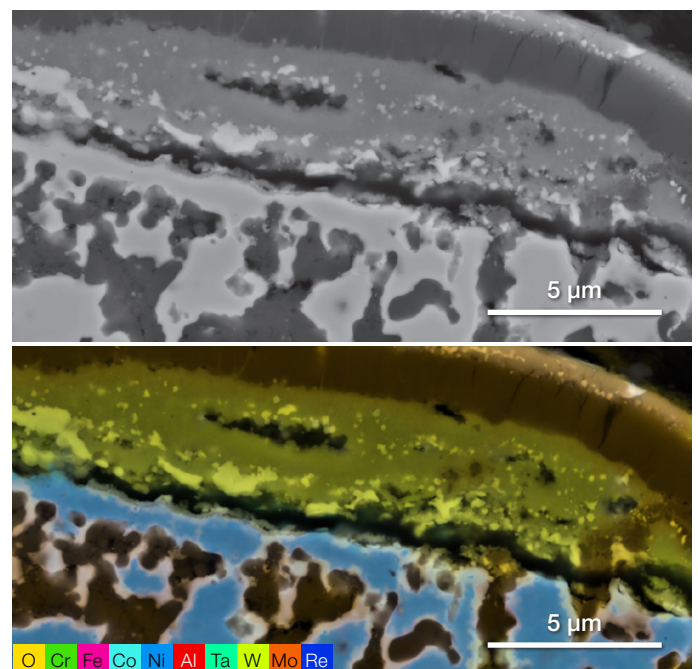
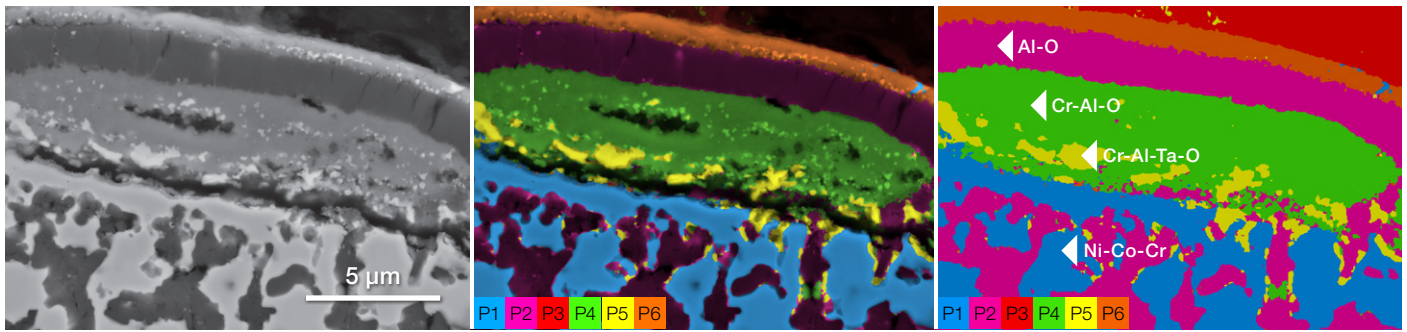


Figure 11. Imaging and ChemiSEM characterization of the material surface.



Name	Phase	Area (μm <sup>2</sup> )	Area %
Base alloy (Ni-Co-Cr)	P1	67.1	26.4
Aluminum oxide	P2	81.3	31.9
Cr-Al-O	P4	58.8	23.1
Cr-Al-Ta-O	P5	13.4	5.3
External layer oxide	P6	15.2	6.0
Embedding material	P3	18.7	7.4

Figure 12. ChemiPhase characterization shows the different phases identified on the sample surface.

Figure 11 shows BSE and ChemiSEM images of the material surface, providing a representative characterization of both the isothermal and thermally cycled materials, as similar features can be observed on both surfaces. Further analysis is, however, required to determine the specific differences between the two samples. The SEM and ChemiSEM images clearly demonstrate that the surface has changed significantly due to high temperature and air exposure. While ChemiSEM analysis offers initial insights into the elements present, it is important to note that a single EDS analysis is insufficient to fully uncover the nature and composition of all the distinct materials, such as the main alloy, oxides, carbides, and other precipitates.

ChemiPhase identified several different materials that were present within the field of view, along with information on their size and area fraction (Figure 12). Note that this analysis does not require users to confirm the elements in each material. However, by quantifying each phase, they could be easily associated with specific materials. (i.e., the yellow phase was identified as chromium-aluminum-tantalum oxide.) While these Ta-containing oxides were found on the surface, the bulk alloy contained tantalum carbides instead. It appears as though the high-temperature oxidizing conditions consumed some of the metallic Cr, Al, and Ta, as well as the associated carbides, to form this new series of oxides at the surface.

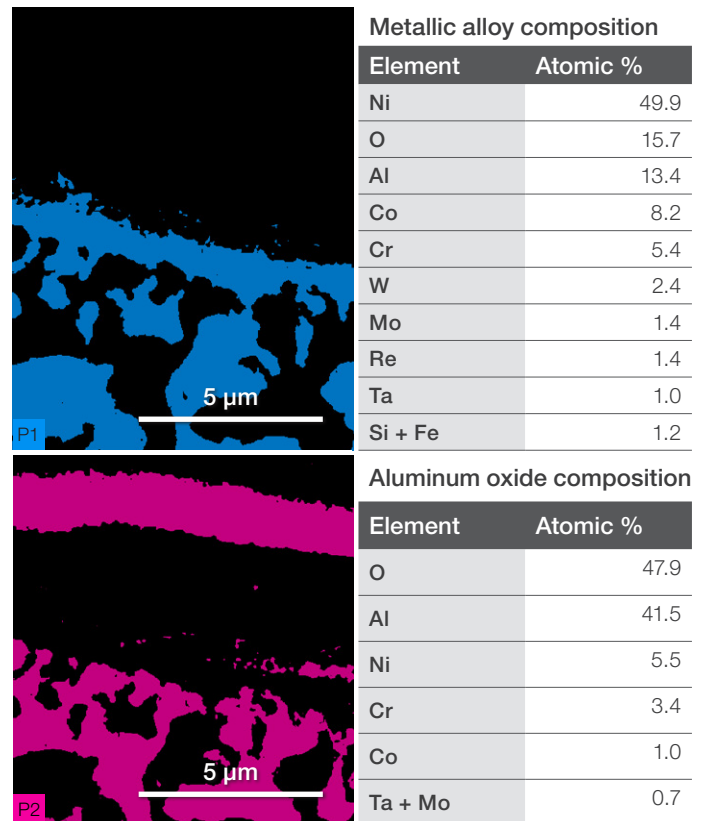


Figure 13. Main alloy (P1) and aluminum oxide (P2) distribution and composition. Data extracted from the ChemiPhase analysis.

The composition of the metallic alloy near the surface (Figure 13) appears to be distinct from both the  $\gamma$  and  $\gamma'$  phases observed in the bulk metal. It can be inferred that heavy oxidation significantly alters the sample surface by robbing the base metal of Al, Cr, and Ta.

## Aluminum nitrides and oxides

Nitrogen in air may also react with the superalloy. The resulting complex alloy can consist of unique species, depending on the oxidation state and elements remaining in that location. Note that neither oxides nor nitrides are formed intentionally in the René N5 alloy, so their presence is not expected to improve mechanical properties. Interestingly, some surface regions did not have as thick an oxidation layer as was observed in previous images. ChemiPhase was used to characterize reaction products in those regions as well.

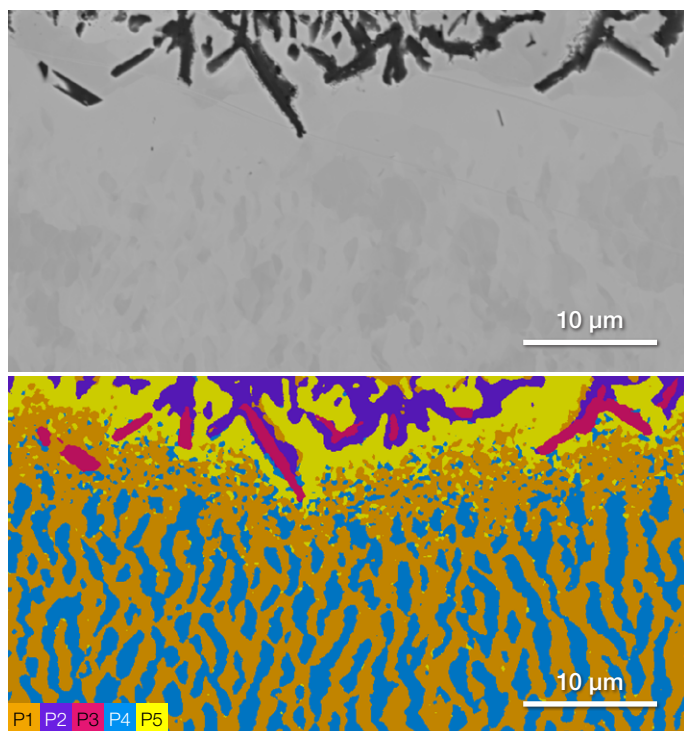


Figure 14. Imaging and ChemiPhase characterization of the area immediately below the sample surface.

Figure 14 displays an SEM image and ChemiPhase map of a surface region with less severe oxidation on the thermally cycled sample. There are many precipitates at the surface, but BSE imaging does not clarify their nature. ChemiPhase analysis, meanwhile, reveals that these are aluminum oxides (P2, purple) and aluminum nitrides (P3, magenta).

Element	P2 Atomic %	P3 Atomic %
O	50.5	21.1
Al	29.2	41.7
N	-	21.5
Ni	12.8	12.0
Cr	3.1	1.6
Co	2.1	1.8
Ta	1.1	-
W + Mo	1.2	0.3

Figure 15. Quantification of the P2 and P3 phases identified in Figure 14 shows that they are aluminum oxides and nitrides.

The change in base metal composition from the bulk to the surface is also evident. The alternating metallic  $\gamma$  (P1, orange) and  $\gamma'$  (P4, blue) phases compose the bulk alloy, but the metallic phase near the surface has a unique composition (P5, yellow). This phase is poor in aluminum due to the formation of the surface precipitates.

## Automated characterization of precipitates

The population of features across both René N5 creep-tested samples was quantified using Thermo Scientific Perception Particle Analysis Software, which utilizes backscattered image thresholding to identify features that are darker than the base metal. Once found, each feature is imaged, measured, and characterized with EDS. Figure 17 shows the aluminum nitride particle maps for the thermally cycled and isothermal samples. The thermally cycled sample yielded 4,592 nitrides whereas the isothermal sample yielded only 228. The surface of the thermally cycled sample is clearly outlined with a dense population of aluminum nitrides. There are likely more nitrides in this sample due to the lower average test temperature and thinner overall oxidation depth. Apparently, the greater oxidation depth of the isothermal sample either blocks nitrogen absorption or binds sufficient aluminum to make aluminum nitride less kinetically favorable.

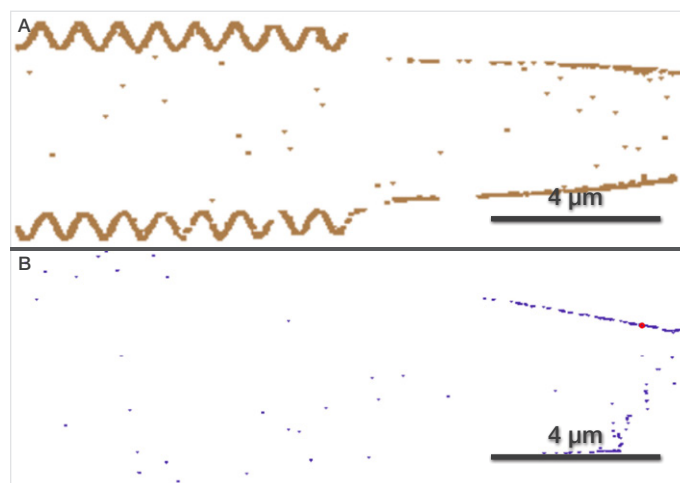


Figure 16. Particle maps showing aluminum nitrides in the thermally cycled (A) and isothermal (B) samples.



The slow growth process used to manufacture single-crystal René N5 alloys can result in small pores, which can then change shape or become deformed when the part is used. Perception Software was used to automatically classify thousands of pores; irregularly shaped, damage-based pores were categorized by an aspect ratio <0.7.

The particle maps shown in Figure 17 reflect the size and location of different features. In both maps, the largest damage-based pores are concentrated at the fracture surface, while smaller pores tend to be found along the single-crystal growth direction.

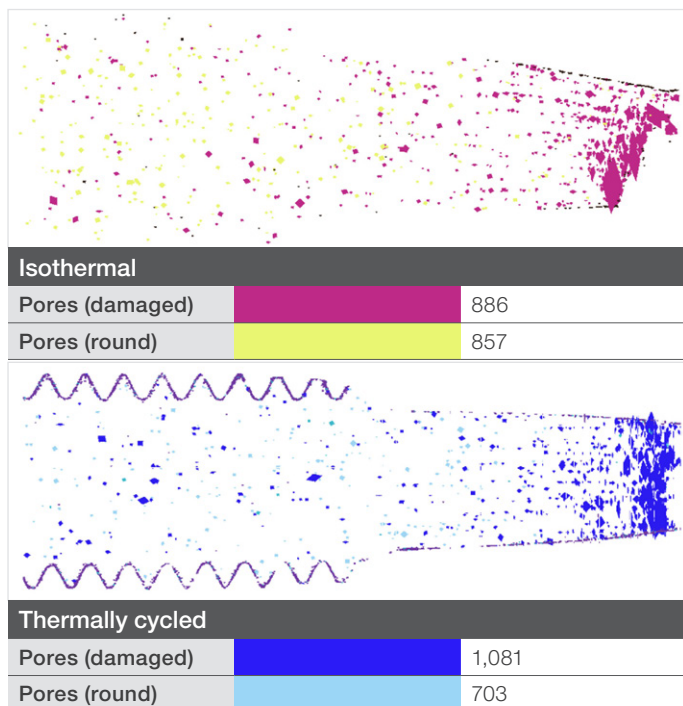


Figure 17. Perception Software particle maps showing selected feature locations.

Many carbides were also captured with Perception Software using a threshold for particles brighter than the base metal. 12 mm<sup>2</sup> regions were selected from within the bulk metal for carbide analysis; both samples yielded similar results.

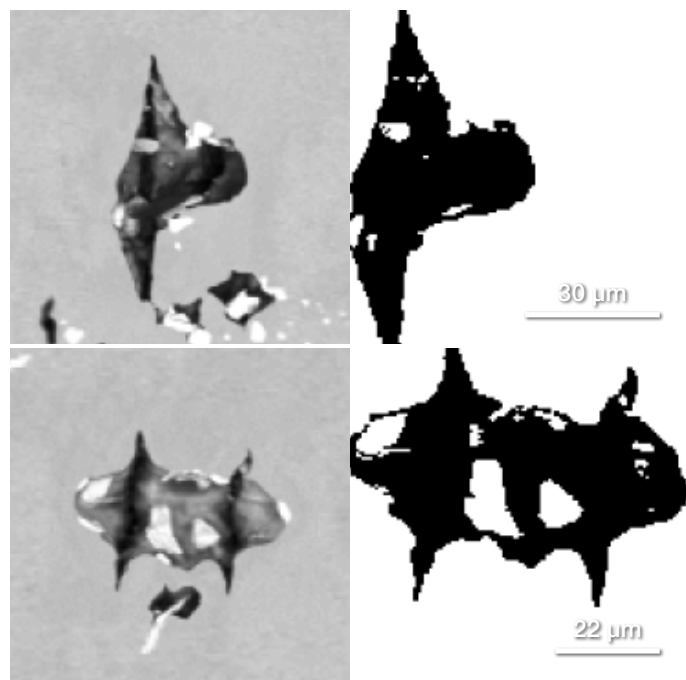


Figure 18. Selected images and threshold masks of damage-based pores, generated automatically in Perception Software.

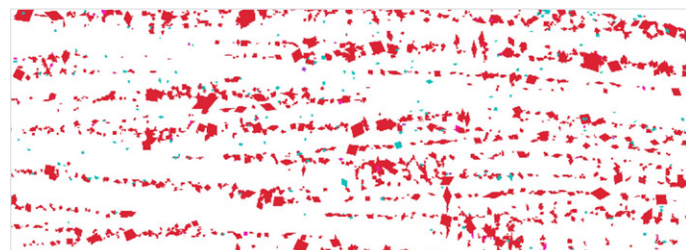
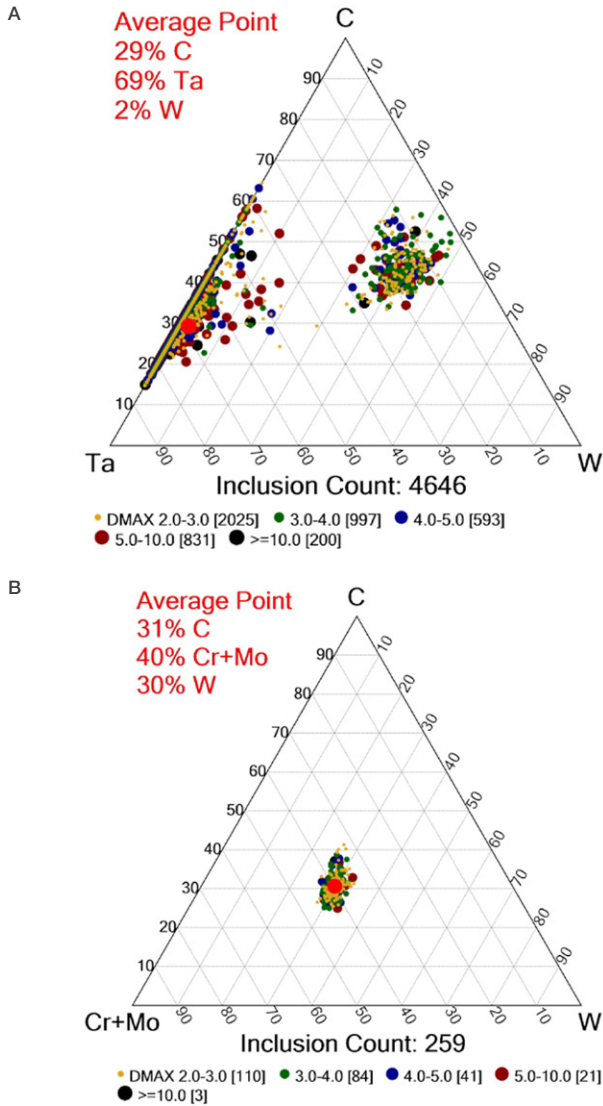


Figure 19. Perception particle map of bright phase carbides in a selected area.

Based on the particle map shown in Figure 19, it appears the larger tantalum carbides (red) form along the growth axis, whereas the smaller Cr-Mo-W carbides (light blue) do not appear to be related to growth. These same particles are shown on ternary diagrams in order to reveal their individual compositions (Figure 20). The two distinct types are shown in Figure 20A, and only the smaller Cr-containing carbides are shown in Figure 20B. Formation of carbides is integral to the high-temperature strength of this alloy, so understanding their size, composition, and location may be useful for new product development.



### Conclusions

The René N5 superalloy is often used in aircraft parts that must withstand high temperatures; understanding its degradation and corrosion at these conditions could reveal failure mechanisms and inform further alloy optimization. In this application note, René N5 was studied with the Apreo ChemiSEM after creep testing under different thermal conditions. Imaging, composition, and particle analysis provided a clear understanding of the metal corrosion products. ChemiPhase analysis quickly identified the composition, amount, and location of each metallic phase as well as all carbides, nitrides, and oxides within the field of view. Automated characterization with Perception Software provided the size, shape, and composition of all carbide, oxide, and nitride particles found within the metal, as well as pores. Overall, this approach can reveal surface corrosion, nitride formation, and the location of damage-based pores.

Figure 20. Automated Perception particle data of bright-phase precipitates reported on ternary diagrams.

Learn more at [thermofisher.com/apreo-chemisem](https://thermofisher.com/apreo-chemisem)